JOURNAL OF MATERIALS SCIENCE 33 (1998) 1529–1540

Processing and characterization of an amorphous Si–N–(O) fibre

G. CHOLLON*, U. VOGT, K. BERROTH
Swiss Federal Laboratories for Materials Testing and Research (EMPA), Ueberlandstrasse 129, CH-8600 Duebendorf, Switzerland

Si–N–(O) fibres were grown according to a high temperature vapour–solid process involving the reaction between SiO and NH_3 on a substrate. The oxygen concentration of the fibres is related to the partial pressures of SiO and NH_3 during fibre growth, depending respectively, on the processing temperature and the ammonia flow rate. The fibres consist of amorphous silicon oxynitride of composition $SiO_{2x}N_{4(1-x)/3}$ ($0.1 < x < 0.2$). They exhibit a large spread in tensile strength. The lowest values (about 1 GPa) correspond to large surface defects caused by intergrowth while the highest values reach 5 GPa for perfect fibres.

The fibres are stable in nitrogen up to 1450 °C (10 h) in terms of composition, structure and mechanical behaviour owing to their high processing temperature (1450 °C) and the nitrogen pressure preventing decomposition. A superficial crystallization into Si_3N_4 is only observed at 1500 °C inducing a moderate decrease of strength. In argon, decomposition starts at 1400 °C yielding gaseous species (SiO and N_2), crystalline Si_3N_4 and free silicon beyond 1400 °C and induce a catastrophic drop of strength. Annealing in oxygen results in a growth of a protective SiO_2 scale, amorphous or partially crystalline at 1400 °C. © *1998 Chapman & Hall*

1. Introduction

Silicon nitride (Si_3N_4) materials are high-temperature structural materials of prime interest because of their excellent properties of thermal shock resistance, corrosion resistance, creep resistance and high strength and stiffness retention at elevated temperature [1]. Silicon oxynitride (Si_2N_2O) is also reported to have excellent refractory properties. Although it was not studied as a pure material but combined with Si_3N_4 and SiC, this material is remarkable for its high strength, low thermal expansion, high thermal shock and abrasion resistance, but especially for its excellent chemical stability in acid, molten non-ferrous metals and air at high temperatures [2]. For these reasons, fibres from the Si–N or the Si–N–O systems are one of the best candidates for metal–matrix composites (MMC) and ceramic–metal composites (CMC) reinforcement. Such fibres should withstand applications in corrosive environments and also severe processing conditions.

Preparation of ceramic fibres by a polymer route is attractive because fine and continuous filaments can be obtained. For instance, amorphous Si–N–(O) fibres were prepared by nitridation of polycarbosilane with ammonia [3] or from the pyrolysis of perhydropolysilazane (PHPS) in ammonia [4]. They are nevertheless subject to a drop of tensile strength [3] or strong Si_3N_4 grain growth after annealing in nitrogen at 1400 °C [5].

Si_3N_4 whiskers can also be used as metal or ceramic material reinforcements. Compared to polymer-based fibres, they exhibit extremely high mechanical properties and structural stability. Furthermore they can be obtained by simple routes and from inexpensive raw materials [6–8]. However, disadvantages of the use of whiskers are their toxicity and the difficulty in incorporating them into matrices.

Alternatively, long Si_3N_4 fibres were also produced according to a process derived from that of the whiskers' production. It involves a vapour–solid reaction of silicon monoxide and nitriding species (e.g. ammonia), resulting in a fibre growth on an appropriate substrate [9]. Long staples of aligned silicon nitride fibres with large diameter (5–15 μm) and length (several centimetres) were obtained, which were more adaptable to the processing of fibrous textures than short whiskers.

A similar gas-phase process was developed by the Swiss Federal Laboratories for Materials Testing and Research (EMPA) in the framework of a Swiss Priority Program for Materials [10, 11]. The aim of this program is to show that heat-resistant silicon-nitride based fibres can be produced in a reproducible manner and according to an inexpensive route. The objective of this paper is to assess the thermal behaviour of these fibres in chemical, structural and mechanical aspects.

---

*Present address: National Institute of Materials and Chemical Research, 1-1 Higashi, Tsukuba, Ibaraki 305, Japan.

0022–2461

2. Experimental procedure

2.1. Fibre synthesis

The overall gas–solid reaction involved in the synthesis of the silicon nitride based fibres can be written as follows

$$3SiO_2 + 4NH_3 \rightarrow Si_3N_4 + 6H_2O \qquad (1)$$

As the solid precursor, amorphous silica ($30\,m^2\,g^{-1}$) was mixed with 10 wt % of titanium powder (150 μm) and about 10 g of this mixture was spread on a silicon carbide substrate. The substrate and the powder precursor were introduced into a horizontal resistance furnace equipped with a silicon carbide tube connected to an ammonia supply. The sample was then heated up to the processing temperature T ($10\,°C\,min^{-1}$, $1400 \leqslant T_a \leqslant 1500\,°C$) for a dwelling time t ($4 \leqslant t \leqslant 16\,h$) under ammonia ($P = 10^5\,Pa$) with a flow rate Q ($50 \leqslant Q \leqslant 150\,l\,h^{-1}$) corresponding to a gas velocity v ($0.0035 \leqslant v \leqslant 0.0105\,m\,s^{-1}$). A dense mat of aligned fibres, grown from the substrate along the gas flow direction was obtained. The position of the fibres within the fibre mat was precisely defined along the three axes (x, y and z) prior to any analysis (Fig. 1). The origin ($x = y = z = 0$) was the edge of the substrate exposed to the gas inlet, at the interface between the substrate and the fibre mat.

2.2. Fibre annealing

In order to investigate the thermal stability of the fibres, annealing treatments of the fibres were performed under various gas atmospheres in an electrical furnace equipped with a silicon carbide tube. Samples were set into a silicon nitride or an alumina boat, heated up ($10\,°C\,min^{-1}$) and maintained at the annealing temperature T_a ($1200 \leqslant T_a \leqslant 1550\,°C$) for a dwelling time t_a of 10 h, under flowing ($P = 10^5\,Pa$) pure argon, nitrogen, oxygen and oxygen/nitrogen mixture (20/80 vol %).

2.3. Characterization techniques

Scanning electron microscopy (SEM) was used to observe the surface and the fracture surface of the fibres (JSM 6300F from Jeol).

Elemental analyses of oxygen and nitrogen were performed on samples of about 5 mg (analyser Leco TC436). The average composition of each sample was calculated after five measurements.

X-ray diffraction (XRD, λCuK_α) patterns were recorded from ground fibres (D500 from Siemens).

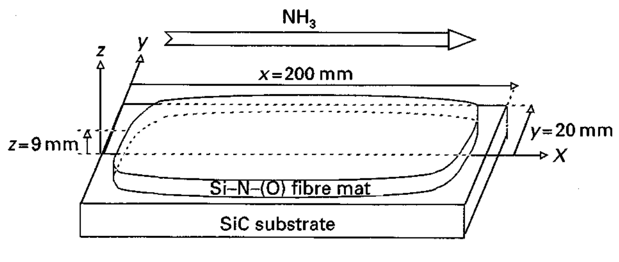

Figure 1 Schematic description of the fibre mat.

The nanostructure of the fibres was studied by high resolution transmission microscopy (HRTEM) (CM20 from Philips). The samples were embedded in an alumina-based cement and cured at about 300 °C. Thin longitudinal specimens were subsequently obtained by polishing and argon milling. The TEM analyses were performed in the bright field (BF) and selected area diffraction (SAD) modes. Local chemical analyses of the TEM samples were carried out by electron energy loss spectroscopy (EELS) and energy dispersive X-ray spectroscopy (EDX).

Solid–state ^{29}Si nuclear magnetic resonance analyses (NMR) in the magic angle spinning conditions (MAS) were performed on fibres and crystalline α-Si_3N_4 (SNE-10 from UBE), Si_2N_2O (Research sample) and SiO_2 (α-quartz) standards. Spectra were acquired at room temperature with a resonance frequency of 79.49 MHz (ASX400 from Bruker). The zircon oxide MAS rotor was filled with 300–500 mg of powder and spun at a rate of 5 kHz during acquisition. The chemical shifts of the ^{29}Si nucleus were referenced to tetramethylsilane (TMS).

The density of the samples was measured by helium-pycnometry (Accupyc 1330 from Micrometretics).

Tensile tests were performed at room temperature on single fibres with a 5 mm gauge length. Individual fibres were carefully removed from a well-defined part of the fibre mat. The two ends of each fibre were glued with cyanocrylate on a paper holder for handling and testing. A mounting system including two grips, a displacement transducer ($\pm$ 1 mm) and a load cell (20 N) was set on a standard tensile tester (Zwick 1478). Tensile tests were then achieved with an elongation rate of $0.05\,mm\,min^{-1}$. The fracture surfaces were examined by SEM to investigate the origin of failure and to measure the diameter of the fibres to calculate their strength.

3. Results

3.1. Influence of the processing conditions

In order to investigate the influence of the main experimental parameters, i.e., the processing temperature (T), time (t) and ammonia flow rate (Q) on the fibres' properties, a work plan was defined. A set of three different values for each of the above parameters was chosen: $T = 1400$, 1450 and 1500 °C; $t = 4$, 8 and 16 h; and $Q = 50$, 100 and $150\,l\,h^{-1}$.

The characteristics of the as-processed fibres (fibre yield, oxygen concentration (C_O), microstructure and average diameter) but also the weight loss of the SiC substrate after each experiment (which was thus found to play a significant part in the fibres synthesis) were investigated fo each processing condition. Because of possible heterogeneities within the fibre mat (discussed in Section 3.2.1), the oxygen concentration, the microstructure and the diameter were measured at a well-defined position, i.e. at the surface, for $x = +100\,mm$ and $y = 0\,mm$ (Fig. 1). The results are presented in Table I and the evolution of the weight loss of the substrate, the fibre yield and the oxygen weight concentration are shown in Figs 2–4.

TABLE I Influence of the processing parameters

T (°C)	Q (NH_3) ($\mathrm{l\,h^{-1}}$)	t (h)	Fibre yield (g)	Substrate weight loss (g)	C_O (wt%)
1400	50	4	0.2	1.27	–
1400	50	16	0.87	2.18	15.6
1400	100	8	0.6	0.98	9.7
1400	150	4	0	0.34	–
1400	150	16	1.05	1.81	7.8
1450	100	16	3.74	5.06	14.2
1450	150	8	1.15	2.7	7.2
1500	50	4	0.86	3.37	16.8
1500	50	8	0.74	6.97	13.3
1500	50	16	2.6	9.68	14.4
1500	150	4	2.42	2.63	9.2
1500	150	16	9.5	12.02	9.3

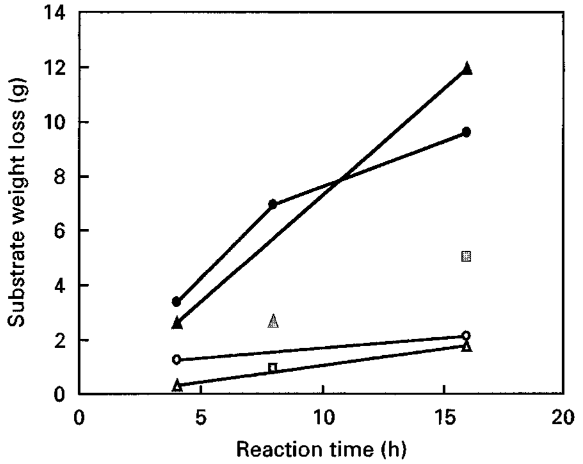

Figure 2 Weight loss of the substrate versus reaction time: (○) $T = 1400\,°C$, $Q = 50\,\mathrm{l\,h^{-1}}$; (□) $T = 1400\,°C$, $Q = 100\,\mathrm{l\,h^{-1}}$; (△) $T = 1400\,°C$, $Q = 150\,\mathrm{l\,h^{-1}}$; (▨) $T = 1450\,°C$, $Q = 100\,\mathrm{l\,h^{-1}}$; (◬) $T = 1450\,°C$, $Q = 150\,\mathrm{l\,h^{-1}}$; (●) $T = 1500\,°C$, $Q = 50\,\mathrm{l\,h^{-1}}$; (▲) $T = 1500\,°C$, $Q = 150\,\mathrm{l\,h^{-1}}$.

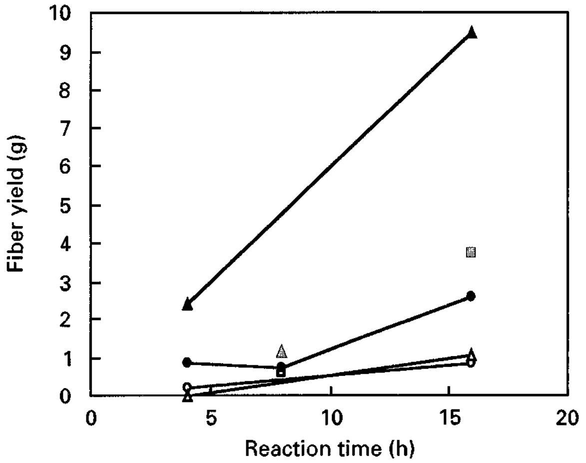

Figure 3 Fibre yield versus reaction time: (○) $T = 1400\,°C$, $Q = 50\,\mathrm{l\,h^{-1}}$; (□) $T = 1400\,°C$, $Q = 100\,\mathrm{l\,h^{-1}}$; (△) $T = 1400\,°C$, $Q = 150\,\mathrm{l\,h^{-1}}$; (▨) $T = 1450\,°C$, $Q = 100\,\mathrm{l\,h^{-1}}$; (◬) $T = 1450\,°C$, $Q = 150\,\mathrm{l\,h^{-1}}$; (●) $T = 1500\,°C$, $Q = 50\,\mathrm{l\,h^{-1}}$; (▲) $T = 1500\,°C$, $Q = 150\,\mathrm{l\,h^{-1}}$.

The diameter of the fibres generally ranges from 1 to 5 μm for the different processing conditions. The relation between the diameter of the fibres and the parameters T, t and Q is extremely complex and would require a larger number of experiments to be discussed.

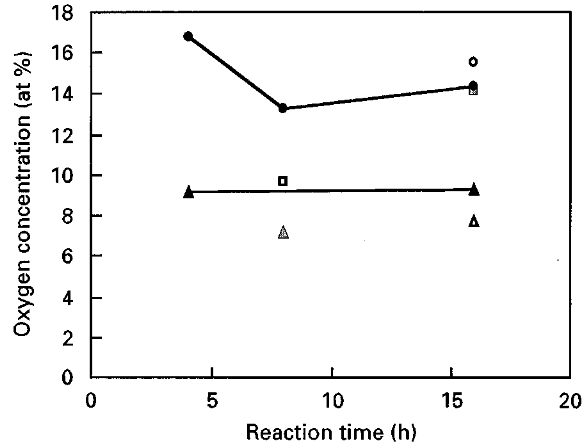

Figure 4 Oxygen concentration versus reaction time: (○) $T = 1400\,°C$, $Q = 50\,\mathrm{l\,h^{-1}}$; (□) $T = 1400\,°C$, $Q = 100\,\mathrm{l\,h^{-1}}$; (△) $T = 1400\,°C$, $Q = 150\,\mathrm{l\,h^{-1}}$; (▨) $T = 1450\,°C$, $Q = 100\,\mathrm{l\,h^{-1}}$; (◬) $T = 1450\,°C$, $Q = 150\,\mathrm{l\,h^{-1}}$; (●) $T = 1500\,°C$, $Q = 50\,\mathrm{l\,h^{-1}}$; (▲) $T = 1500\,°C$, $Q = 150\,\mathrm{l\,h^{-1}}$.

Except for very high temperature and long reaction times ($T = 1500\,°C$ and $t = 16\,h$) where weak peaks due to α-Si_3N_4 were observed, the XRD analyses of all the fibres only showed two very broad peaks corresponding to an amorphous state.

As shown in Fig. 2, a significant weight loss of the SiC substrate was observed after each run. It increases almost linearly with the reaction time whatever the temperature (T) and the ammonia flow rate (Q). The rate of weight loss is considerably enhanced by T but not influenced by Q.

The fibre yield increases continuously with time whatever T and Q (Fig. 3). It tends to increase with T for a given value of Q and reaction time. Whereas there is almost no influence of the ammonia flow rate on the kinetics at low temperature ($T = 1400\,°C$), an increase of Q from 50 to $150\,\mathrm{l\,h^{-1}}$ at high temperature ($T = 1500\,°C$) leads to a much higher yield.

For given values of Q and T, the oxygen concentration remains almost constant for different reaction times (Fig. 4). It decreases with increasing Q and is almost not influenced by T.

3.2. Characterization of the fibres in the as-processed state

3.2.1. Characterization of the fibre mat

The properties of the as-processed fibre mat were investigated for the following set of parameters, resulting from the optimization of the processing conditions (Section 3.1): $T = 1450\,°C$, $t = 16\,h$ and $Q = 125\,\mathrm{l\,h^{-1}}$.

The morphology, the diameter and the chemical composition were assessed along the gas flow direction (the logitudinal axis x) and the depth of the mat (z axis).

The maximal diameter of the fibres at different places in the mat is shown in Fig. 5. It clearly appears that the diameter gradually decreases along the x axis whatever the depth in the mat. The diameter of the

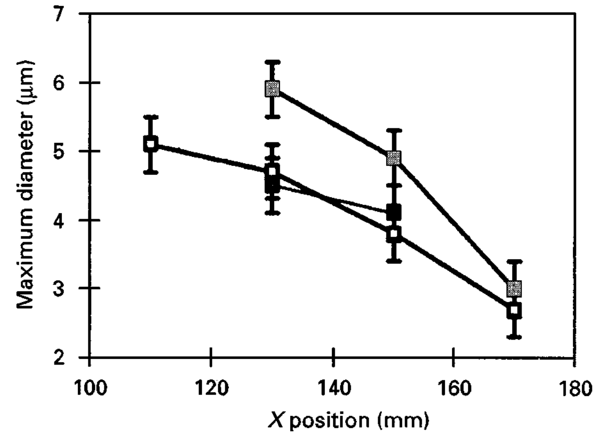

Figure 5 Fibre diameter versus x and z positions in the fibre mat. (■) $z = 3$ mm; (▨) $z = 6$ mm; (□) $z = 9$ mm.

upper fibres is also thinner than that from the centre part. The morphology of the fibres strongly depends on the position of the fibres within the bundle. A large number of kinked and curved fibres are observed at the gas inlet side of the bundle while mostly straight fibres are present at the gas outlet side. Furthermore, for a given position, a larger number of coiled, disoriented and tangled fibres are observed in the depth.

The oxygen content significantly increases along the x axis and from the upper part to the bottom of the mat (Fig. 6a). There is a reverse evolution of the nitrogen content with x and z (Fig. 6b).

For all the different parts of the bundle, XRD pattern showed only indications of an amorphous state (Fig. 7a).

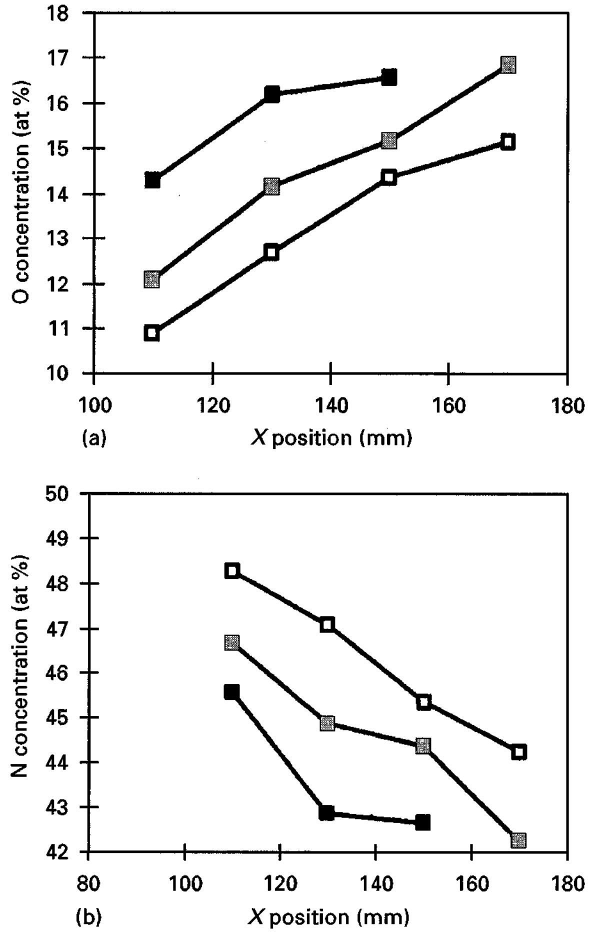

Figure 6 Oxygen (a) and nitrogen (b) concentrations versus x and z positions in the fibre mat. (■) $z = 3$ mm; (▨) $z = 6$ mm; (□) $z = 9$ mm.

3.2.2. Characterization of individual fibres

The following analyses were performed on fibres taken from a zone of the fibre mat defined by $x = (100; 140)$ mm, $y = (-15; 15)$ mm and $z = (3; 9)$ mm. The fibres' properties were assumed to be homogeneous within this domain of the mat.

The TEM analyses confirmed the amorphous character of the fibres. High resolution analyses only revealed a contrast typical of an amorphous material (Fig. 8). The SAD pattern showed no distinct diffraction spot but only diffuse scattered electrons. No gradient of composition, from the surface to the bulk of the fibre was found by EELS whereas XPS analyses coupled with argon milling revealed a slightly higher O/N ratio at the surface of the fibre (with a thickness of only about 10 nm).

The ^{29}Si-NMR spectra of the fibres compared to the crystalline standards are shown in Fig. 9. All the crystalline compounds show well-defined and narrow resonance peaks. The spectrum of the α-Si_3N_4 powder shows two narrow peaks at -50.4 and -48.2 p.p.m. with almost the same intensity and full width at half height (FWHH), in good agreement with spectra already presented in the literature for similar materials [12, 13]. The spectrum of the Si_2N_2O research sample shows two peaks at -62.3 p.p.m. (intense) and -49.0 p.p.m. (weak). The former is characteristic of the crystalline Si_2N_2O phase [12, 13] whereas the latter shows the presence of residual crystalline Si_3N_4. The spectrum of the quartz sample exhibits a characteristic single narrow peak at -107.5 p.p.m.

The ^{29}Si-NMR spectrum of the fibres shows a single very broad and asymmetric peak from -85 to -35 p.p.m., along with all the peak positions from the spectra of crystalline Si_3N_4 and Si_2N_2O. Since the spinning side band (s.s.b.) of the main ^{29}Si-NMR peak, observed from -140 to -95 p.p.m. for a spinning rate of 5 kHz (Fig. 9) may interfere with a peak caused by the eventual presence of a SiO_2 phase (at about -110 p.p.m.), a further acquisition was made with a lower spinning rate. It was thus ensured that no line characteristic of a SiO_2 phase was detectable on the spectrum of the fibres.

The density of the fibres measured by helium pycnometry was $d = 3\,\mathrm{g\,cm^{-3}}$.

Individual fibres (about 30 specimens) were carefully pulled out from the same zone of the mat and submitted to tensile tests. The tensile strengths are shown versus the fibre diameter in Fig. 10 and in a Weibull plot in Fig. 11.

The fibres exhibit a large spread in tensile strength values. For a gauge length of 5 mm and diameters of 4.5–6 μm, σ^R currently ranges from 1 to 5 GPa. The maximum strength values are obtained for small

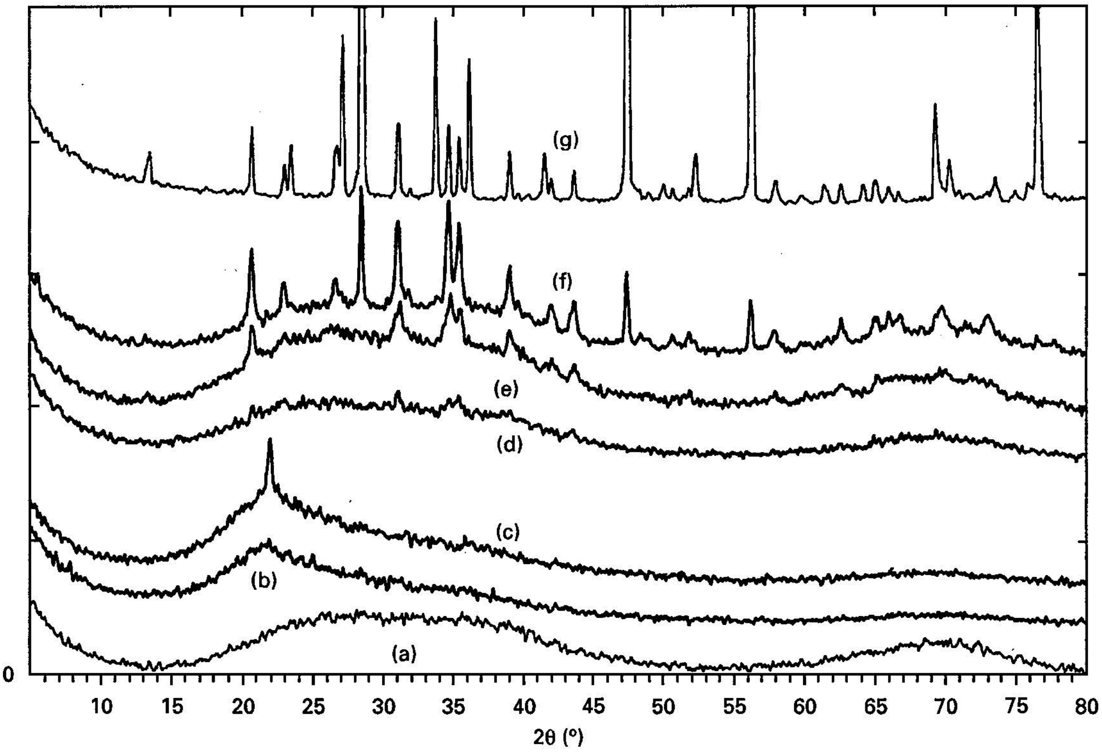

Figure 7 XRD pattern of the as-processed and annealed ($t_a = 10$ h) fibres. (a) as-processed; (b) $T_a = 1350$ °C in oxygen; (c) $T_a = 1400$ °C in oxygen; (d) $T_a = 1500$ °C in nitrogen; (e) $T_a = 1400$ °C in argon; (f) $T_a = 1450$ °C in argon; (g) $T_a = 1500$ °C in argon.

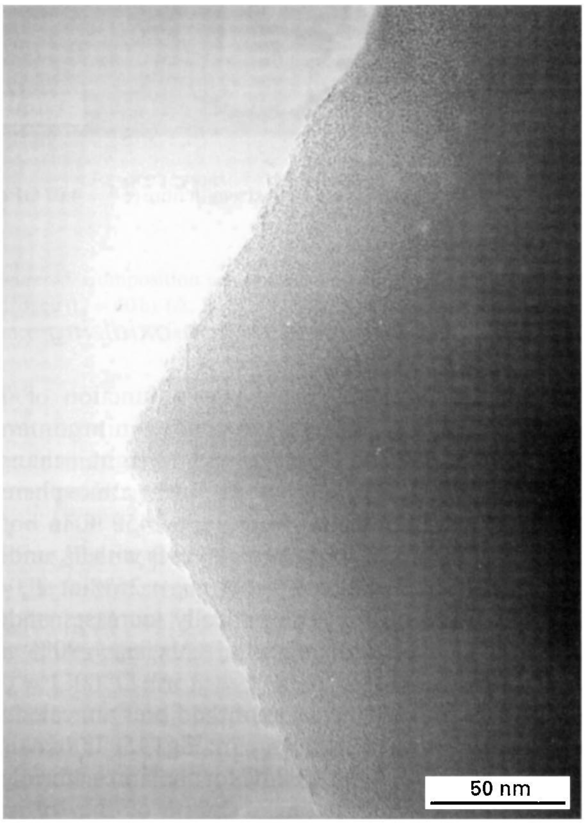

Figure 8 High resolution TEM micrograph of the as-processed fibre.

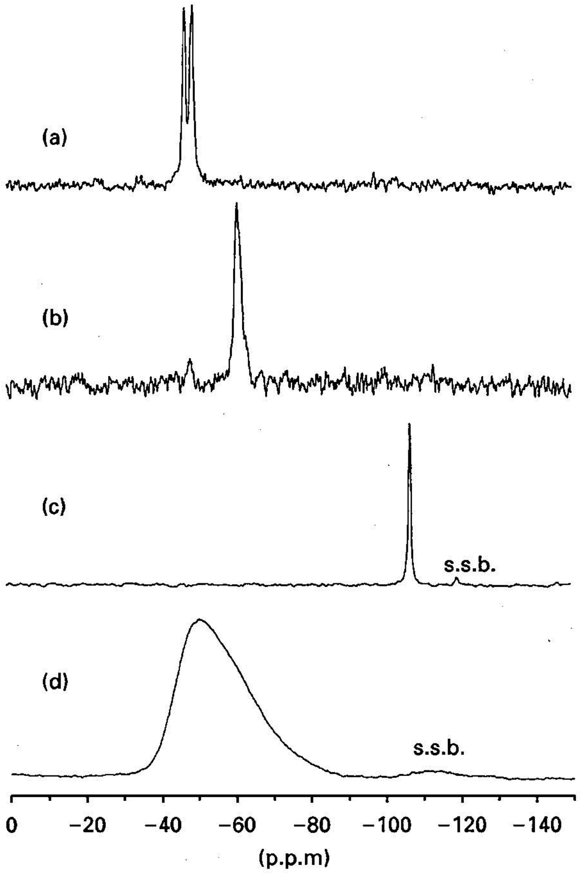

Figure 9 Silicon-29 MAS NMR spectra of (a) α-silicon nitride, (b) silicon oxynitride, (c) α-quartz, (d) the Si–N–(O) fibres (s.s.b. are spinning side bands).

diameters. The strength distribution plotted in a Weibull diagram is not strictly linear. The characteristic strength (for a probability of failure of $P^R = 63\%$) is $\sigma^R = 2.31$ GPa and the Weibull modulus $m = 2.76$. SEM analyses of the failure surfaces showed that the failure was always initiated from the surface of the

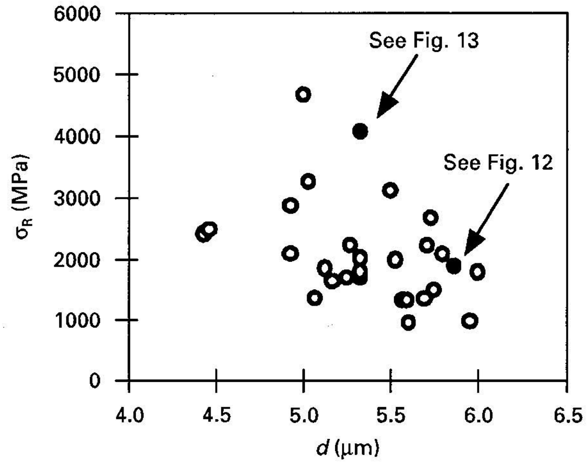

Figure 10 Failure strength of the fibres versus diameter.

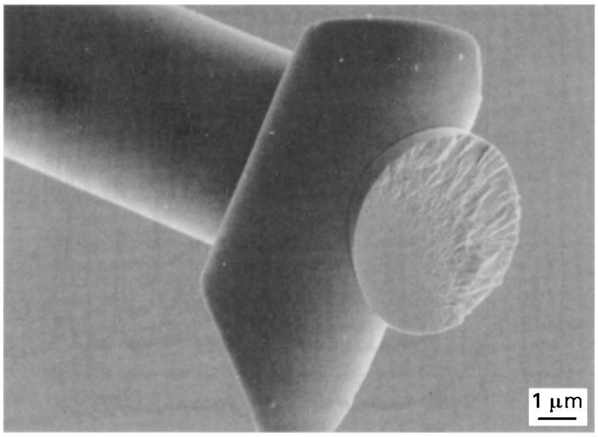

Figure 12 Fracture surface of a low strength fibre ($\sigma^R = 1.88$ GPa).

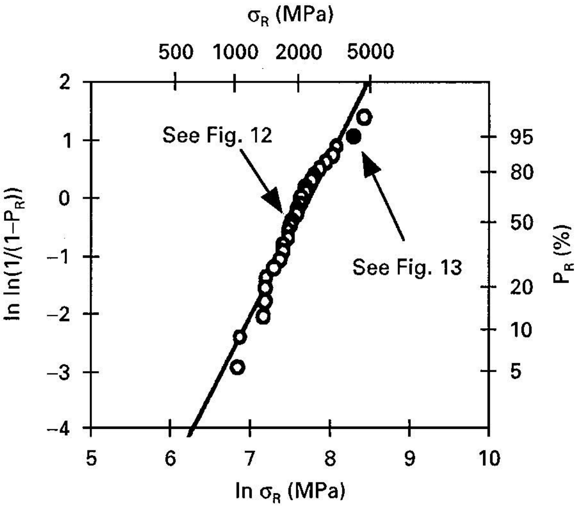

Figure 11 Weibull plot of the failure strength of the fibres.

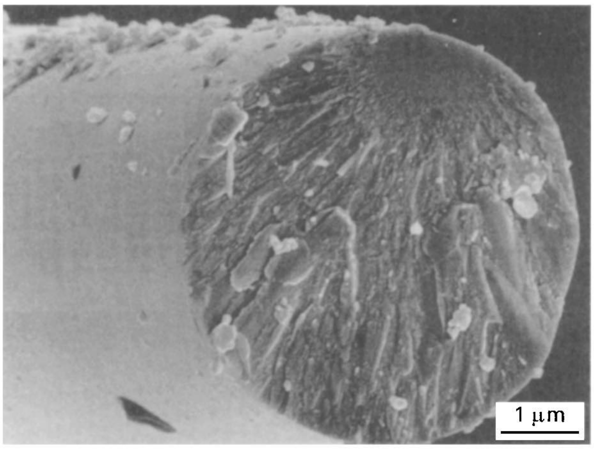

Figure 13 Fracture surface of a high strength fibre ($\sigma^R = 4.07$ GPa).

fibre. Furthermore, for a large number of specimens, the failure was induced by large surface defects like kinks or cross-linking (Fig. 12). It is noteworthy that fibres with such type of flaws can nevertheless reach a strength of about 2 GPa. The failure surface of such a fibre clearly shows a mirror zone surrounding the origin of failure, i.e. the sharp edge at the intersection of the two fibres. The highest strengths achieved reached values up to 5 GPa. They were obtained for fibres with a smooth surface, a small cross-section and without large defects. They can be distinguished from the other fibres by a small mirror zone and no apparent flaw (Fig. 13).

3.3. Fibres after annealing

In order to study the influence of thermal treatments on the fibres, samples with similar starting properties were investigated. The samples were thus taken from a position in the fibre mat defined by $x = (100; 140)$ mm, $y = (-15; 15)$ mm and $z = (3; 9)$ mm. The gas inlet side and the lower parts were rejected because of too large a number of faulted fibres and/or too high an oxygen content. For a given annealing atmosphere, the samples were taken from the same fibre mat.

3.3.1. Fibres annealed in non-oxidizing atmospheres

The weight losses ($-\Delta m/m_0$) as a function of T_a are shown in Fig. 14 for fibres treated in argon and nitrogen. There is almost no weight change for $T_a \leqslant 1400\,°C$ ($t_a = 10$ h) in both atmospheres. A weight loss is observed from $T_a = 1450\,°C$ in both cases. It slightly and gradually increases with T_a under nitrogen, up to a value of $-\Delta m/m_0 = 25\%$ at $T_a = 1550\,°C$. Conversely, it dramatically increases under argon to a value of about $-\Delta m/m_0 = 90\%$ at $T_a = 1500\,°C$.

The chemical composition of the fibres annealed in argon and nitrogen is shown in Fig. 15. It remains unchanged up to $T_a = 1500\,°C$ for the fibres annealed in nitrogen while a strong decrease of the oxygen content from $T_a = 1400\,°C$ to 1500 °C is observed for the fibres annealed in argon.

Almost no change of the amorphous state of the material is noticed for the fibres annealed in nitrogen except weak peaks ($2\theta = 31.0$, 34.6 and 35.3°) for $T_a = 1500\,°C$, which can be assigned to α-Si_3N_4 (Fig. 7d). The fibres remain amorphous in argon for $T_a \leqslant 1300\,°C$ and weak peaks assigned to α-Si_3N_4 appear for $T_a = 1400\,°C$. For $T_a = 1450\,°C$, the

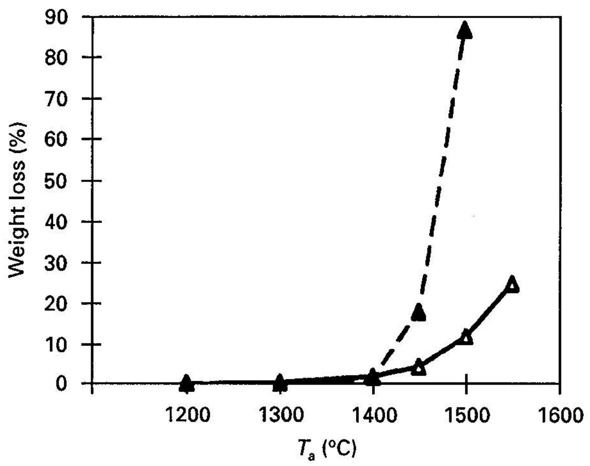

Figure 14 Weight loss versus annealing temperature in argon (▲) and nitrogen (△) (t_a = 10 h).

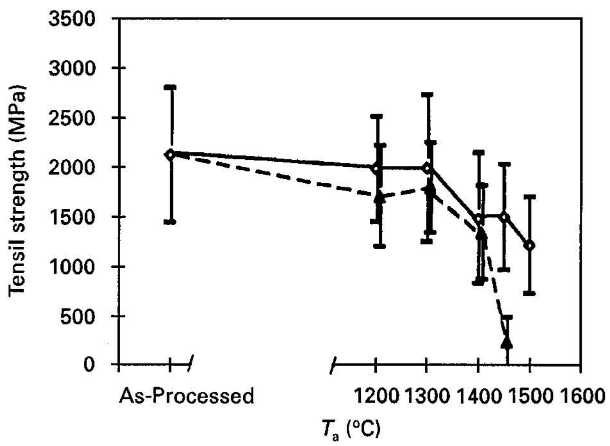

Figure 16 Failure strength versus annealing temperature in argon (▲) and nitrogen (◇) (t_a = 10 h).

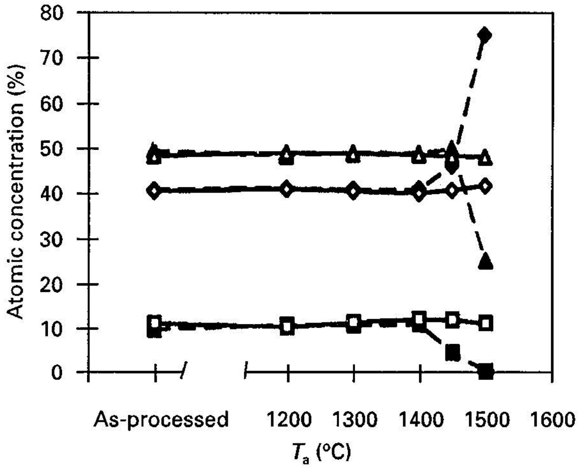

Figure 15 Composition versus annealing temperature in argon and nitrogen (t_a = 10 h). (△, ▲) N concentration in N_2 and Ar; (◇, ◆) Si concentration in N_2 and Ar; (□, ■) O concentration in N_2 and Ar.

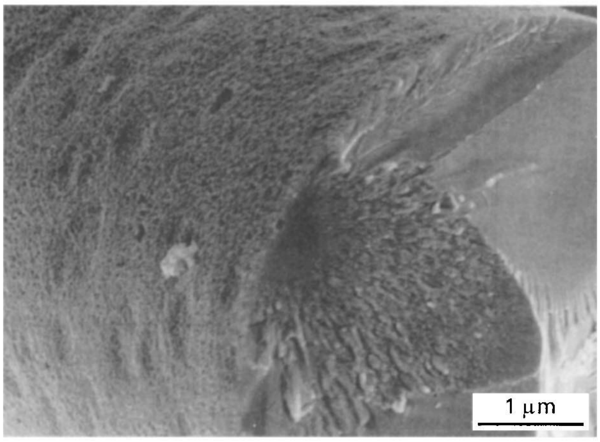

Figure 17 Fracture surface of a fibre annealed 10 h in nitrogen at 1500 °C (σ^R = 1.82 GPa).

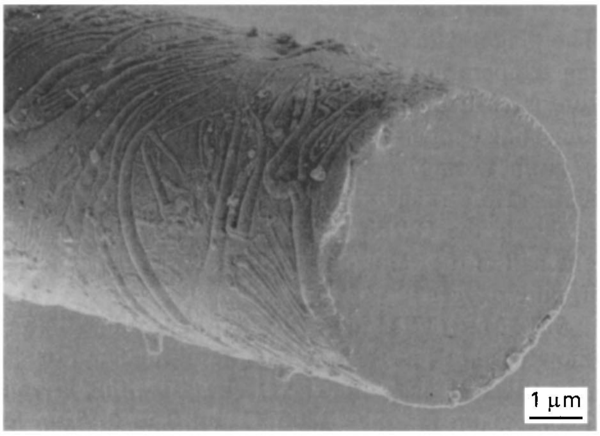

Figure 18 Fracture surface of a fibre annealed 10 h in argon at T = 1400 °C (σ^R = 1.22 GPa).

crystallization of α-Si_3N_4 proceeds simultaneously to the formation of free silicon, as shown by the very sharp peaks at 2θ = 28.4, 47.3 and 56.1° (Fig. 7f). For T_a = 1500 °C, the material only consists of a mixture of free silicon, β-Si_3N_4 and α-Si_3N_4 (Fig. 7g).

The failure strength of the fibres versus the annealing temperature is shown in Fig. 16. The strength of the fibres annealed in nitrogen is unchanged up to T_a = 1300 °C (for t_a = 10 h). A slight and gradual decrease of σ^R is observed from this temperature to T_a = 1500 °C. The strength of the fibres annealed in argon is also slightly reduced for T_a = 1400 °C. It is worthy of note that the effective strength of the latter fibres is probably lower, because a significant number of specimens were broken before testing, owing to their extreme brittleness. For T_a = 1450 °C, the fibres treated in argon were too brittle to be tested. Their strength is thus assumed to be lower than 0.5 GPa.

The failure surfaces of tensile tested fibres were analysed. The fibres treated at T_a = 1500 °C in nitrogen still exhibit a fracture surface which is typical for an amorphous material. Some of these fibres show a rough surface after annealing, for instance the one shown in Fig. 17, where the failure was induced by a surface flaw caused by the heat treatment. The bulk of the fibres annealed at T_a = 1400 °C in argon is also unchanged. Conversely, they show a heterogeneous degradation of their surface, with a dendritic structure (Fig. 18). The degradation reaches the whole bulk for T_a = 1450 °C (Fig. 19).

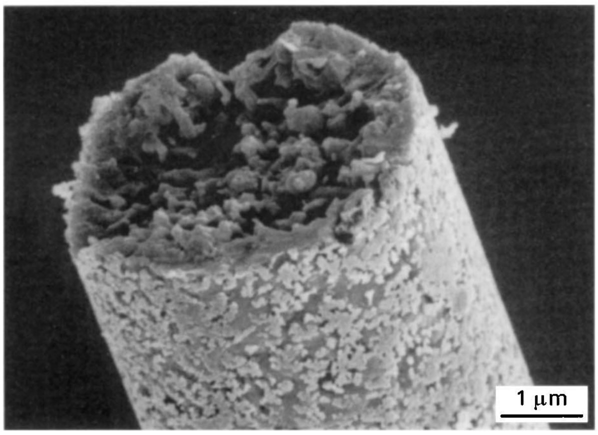

Figure 19 Fracture surface of a fibre annealed 10 h in argon at $T = 1450\,°C$ ($\sigma^R < 0.5\,GPa$).

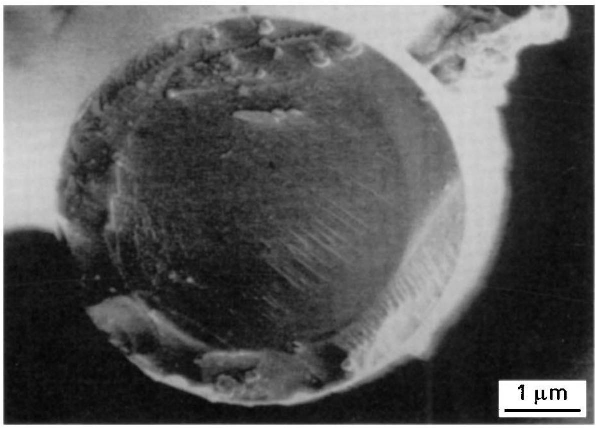

Figure 21 Fracture surface of a fibre annealed 10h in oxygen at $T = 1400\,°C$.

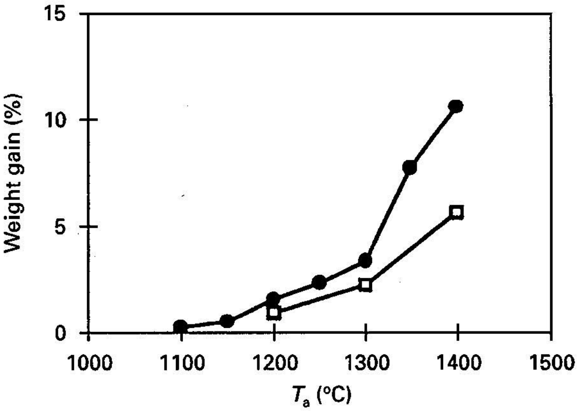

Figure 20 Weight gain versus annealing temperature in pure oxygen (●) and in 20 vol% O_2 + 80 vol% N_2 (□).

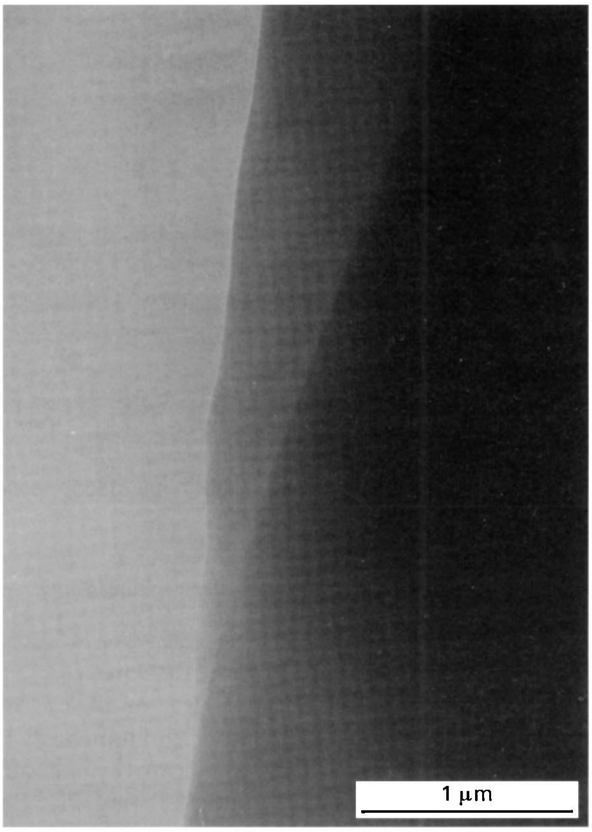

Figure 22 TEM bright-field micrograph of a fibre annealed 10 h in oxygen at $T = 1400\,°C$.

3.3.2. Fibres annealed in oxidizing atmosphere

The weight gain ($\Delta m/m_0$) as a function of the annealing temperature in oxygen or oxygen/nitrogen mixture is plotted in Fig. 20. $\Delta m/m_0$ increases with the annealing temperature in both cases. Furthermore, for a given testing temperature and within the whole temperature range, the weight gain of the fibres annealed in the O_2/N_2 mixture (25 vol% O_2) is about one half of the value obtained for the fibres annealed in pure oxygen.

SEM and TEM analyses of the oxidized fibres showed a scale at their surface, resulting from oxidation (Figs 21 and 22). The thickness of this layer is 0.80–0.85 μm for $T_a = 1400\,°C$ and 0.50–0.55 μm for $T_a = 1350\,°C$. XPS analyses achieved for the fibres oxidized at 1400 °C showed that the layer consists of pure SiO_2, at least from the surface to a depth of 40 nm. Only silicon and oxygen were detected by EDX and EELS within this layer, with a steep chemical gradient at the oxide/fibre interface.

The silica layer remains amorphous up to 1350 °C as shown by XRD analyses (Fig. 7b). The intensity of the broad amorphous silica peak at $2\theta = 18$–$24°$ gradually increases with T_a. A weak but sharp peak at $2\theta = 21.6°$ appears at 1400 °C, indicating the starting of the crystallization of silica into cristobalite (only the α form, metastable at room temperature, is visible on the XRD pattern) (Fig. 7c). Crystalline oxide layer domains could be seldom seen by SEM analysis.

4. Discussion

4.1. The as-processed fibres

The amorphous structure of the fibres is well established by the XRD, TEM and NMR analyses. The absence of Bragg diffraction peaks denotes the extremely low crystalline order (probably lower than 1 nm). The absence of well defined peaks on the NMR spectrum is indicative of a large spread in chemical bond length and angle. The extremely large band observed on the NMR spectrum is due to the substitution of nitrogen atom(s) from the Si–N_4 tetrahedral

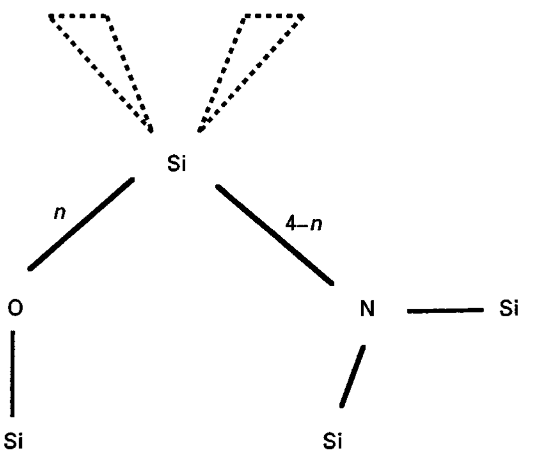

Figure 23 Schematic description of the tetrahedral environment of silicon atoms in the fibre (Si–$N_{4-n}O_n$ with $n = 0, 1, \dots, 4$).

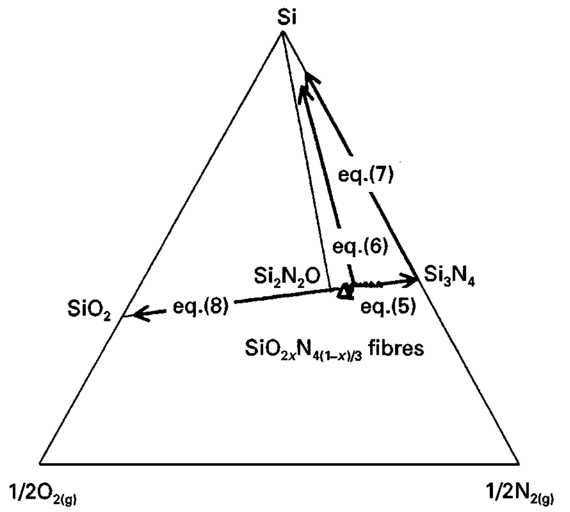

Figure 24 Phase diagram of the Si–N–O system showing the composition of the as-processed and annealed fibres.

environment in Si_3N_4 by oxygen atom(s), forming mixed Si–$N_{4-n}O_n$ environments (with $n = 0, 1, \dots, 4$) (Fig. 23). The contribution of a SiO_2 phase on the global composition of the fibre has been dismissed by XPS, NMR and TEM analyses. The oxygen is therefore homogeneously distributed through the fibre under the form of a single amorphous silicon oxynitride phase where the silicon atoms have a mixed Si–$N_{4-n}O_n$ tetrahedral environment ($n = 0, 1, \dots, 4$) and the oxygen and the nitrogen atoms are respectively bonded to two and three silicon atoms. It can be easily shown that its chemical composition can be defined by the only parameter x, i.e. $SiO_{2x}N_{4(1-x)/3}$ within the case of the fibres $0.1 < x < 0.2$ (8–17 at % of oxygen). This theoretical domain of composition corresponds quite well to the experimental domain, i.e., a composition located between Si_3N_4 ($x = 0$) and Si_2N_2O ($x = 0.25$) on the Si–N–O phase diagram (Fig. 24).

The density of the fibres is remarkably high compared to that of their polymer derived counterparts ($d = 2.4\,\mathrm{g\,cm^{-3}}$ for the PHPS-derived fibre) [4] and almost equal to the theoretical value calculated from the rule of mixture ($d = 3.1\,\mathrm{g\,cm^{-3}}$). Such a high density is an indication of the absence of nanoporosity within the structure of the fibre.

Owing to their amorphous state, small diameter and smooth surface, the fibres have a high potential strength. However, the mean strength is limited by surface flaws caused by intergrowth, inducing local stress concentrations.

4.2. Fibre processing

The synthesis of silicon nitride and silicon oxynitride from the reaction of silica and ammonia has been studied for many years [14–19]. The nitridation of amorphous silica into amorphous silicon oxynitride is a relatively low-temperature process [14–17]. It is characterized by low kinetics and the conversion is generally limited to the surface of the silica. The process requires the presence of NH_3 rather than N_2 for its high nitriding potential and reducing properties. Furthermore, the decomposition of ammonia occurring above 800 °C yields, in addition of N_2 and H_2, transient reactive NH_x radicals ($0 < x < 3$). It is therefore suggested to be essential for the nitridation process [17].

The synthesis of the Si–N–(O) fibres, as for crystalline Si_3N_4 powders or whiskers, is a higher-temperature process [17–19]. In the case of the present fibres, the growth of the silicon oxynitride structure on a substrate does not only require the providing of NH_3 or (NH_x) but also silicon- and oxygen-rich gaseous species. For thermodynamic considerations, SiO is thought to be involved in the fibre growth process (though it could not be detected by mass spectrometry because of its instability at low temperature), as already suggested by other authors [17–19]. SiO can be generated from the reduction of silica by molecular or atomic hydrogen resulting from the degradation of ammonia according to Equation 2

$$SiO_2 + H_2 \rightarrow SiO + H_2O \qquad (2)$$

It can also be formed by the reduction of silica by the silicon carbide substrate, consistent with the high temperature process (Equation 3) [20]

$$SiO_2 + SiC \rightarrow SiO + CO \qquad (3)$$

The last assumption is supported by the significant weight loss of the substrate, enhanced by temperature only. Assuming that NH_3 is the only nitriding specie for simplification reasons, the synthesis reaction can be tentatively written by Equation 4

$$SiO + [4(1-x)/3]NH_3 \rightarrow SiO_{2x}N_{4(1-x)/3} + (1-2x)H_2O + H_2 \qquad (4)$$

SiO being generated from the silica or at the interface between the silica and the SiC substrate (Equations 2 and 3) and NH_3 (and/or NH_x) being provided by the gas flow, according to two opposite gas fluxes through the fibre mat (Fig. 25).

The interpretation of the influence of the processing parameters (Q and T) on the yield and the oxygen concentration of the fibres is easy from Equation 2 and

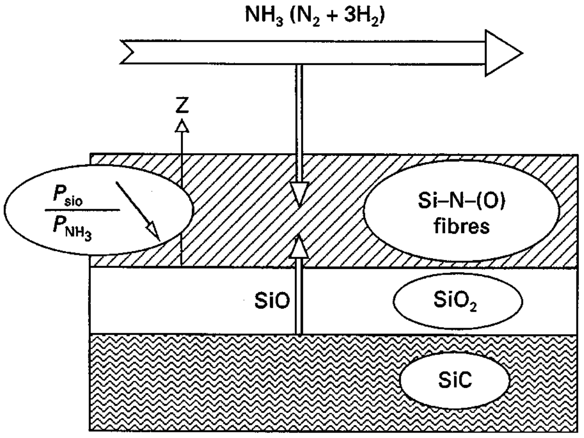

Figure 25 Schematic description of the mechanism of fibre growth.

Fig. 25. The decrease of the oxygen concentration of the fibre mat along the z axis can be explained by the gradient of the partial pressures of both SiO and NH_3 fluxes through the mat. The ratio P_{SiO}/P_{NH_3} decreases along the z axis resulting in a gradual decrease of x (or C_O) (Equation 4, Fig. 25). For similar reasons, the decrease of the ammonia partial pressure along the gas flow direction, owing to its thermal decomposition and its reaction with SiO (Equation 4), results in an increase of C_O along the x axis.

The complex behaviour of the fibre yield with T and Q is thought to be related to the incompatibility of the respective domains of thermal stability of SiO and NH_3. Because of the high processing temperature range, the effective partial pressure of NH_3 on the substrate is extremely low as the major part of the gas flow is composed of H_2 and N_2 (the thermodynamic equilibrium is, however, not reached because of the high gas flow above the substrate). The change of the processing temperature in the range 1400–1500 °C is therefore much more influential for the magnitude of the SiO partial pressure [20]. Because of the low value of P_{SiO} at $T = 1400\,°C$, the formation of SiO is thought to be the limiting step for the kinetics of Equation 4. Thus, the change of the ammonia flow rate (Q) has only a little influence on the fibre yield, as shown in Fig. 3. Conversely, P_{SiO} is considerably higher at $T = 1500\,°C$ and the controlling step is thought to be in this case providing of ammonia. For this reason, at such a high temperature, an increase of Q results in a much higher fibre yield (Fig. 3).

4.3. Thermal stability in nitrogen

The chemical composition and the amorphous state of the fibres are both almost unchanged after annealing at high temperature in a high nitrogen pressure. However, a slight crystallization simultaneous to a superficial degradation occurs for $T_a = 1500\,°C$ ($t_a = 10\,h$) which creates new surface flaws and consequently induces a slight decrease of the fibres' failure strength. The fibres nevertheless retain high properties with respect to their polymer derived Si–N–O counterparts [3, 5]. The decomposition at high temperature in a nitrogen flow (100 kPa) yields α-Si_3N_4 and an evolution of SiO and N_2 according to Equation 5 (Fig. 24). It consequently results in a weight loss of the fibres depending on the rate of Equation 5 and their starting oxygen content (x)

$$SiO_{2x}N_{4(1-x)/3} \rightarrow [(1-2x)/3]Si_3N_4 + 2x\,SiO + (2x/3)N_2 \quad (5)$$

Despite the significant weight loss recorded at 1500 °C, the composition of the fibre remains stable. This feature suggests an additional degradation mechanism to the inherent fibre decomposition, e.g. an active oxidation process, which would result in a weight loss without any chemical change of the residues [21]. This assumption is supported by the occurrence of superficial pittings observed at higher decomposition rates ($T_a > 1500\,°C$, $t_a > 10\,h$). Furthermore, the heterogeneous recrystallization of α-Si_3N_4 observed mainly at the periphery of the bundle and on the crucible (probably achieved through a gas transport process [22]) could also explain the apparent stability of the chemical composition of the fibres.

4.4. Thermal stability in argon

The thermal stability of the fibres is significantly lower in argon than in nitrogen. The decomposition inducing again a crystallization of α-Si_3N_4 at $T_a = 1400\,°C$, takes place first at the surface of the fibre. Similarly to the above, the decomposition rate of the fibres is not homogeneous. The fibres at the periphery of the bundle are more degraded than those from the inner part. The higher partial pressures of SiO and N_2 in the latter case prevent decomposition and, consequently, the decrease of failure strength. The degradation reaches the bulk for $T_a > 1400\,°C$, inducing a catastrophic drop of strength. The amount of crystalline phases (α-Si_3N_4 and subsequently free silicon and α-Si_3N_4 in higher proportions) gradually increases with T_a detrimentally to the amorphous phase (Fig. 7). This feature is consistent with thermodynamic calculations and Knundsen cell mass analyses of Si_3N_4 and Si_2N_2O in vacuum [23, 24]. The overall decomposition of the fibre in argon (or vacuum) can thus be described by Equation 6 (Fig. 24)

$$SiO_{2x}N_{4(1-x)/3} \rightarrow (1-2x)Si + 2xSiO + [2(1-x)/3]N_2 \quad (6)$$

The transient formation of Si_3N_4 which is experimentally observed, could be explained by kinetic reasons [24]. The decomposition of the fibre might obey first Equation 5 followed by the decomposition of the resulting Si_3N_4 residues according to Equation 7 (Fig. 24)

$$Si_3N_4 \rightarrow 3Si + 2N_2 \quad (7)$$

4.5. Thermal stability in oxygen

Like many silicon-based materials, annealing treatments of the fibres in oxygen or in an oxygen/nitrogen mixture result in the growth of a silica layer at the surface of the fibre [25–30]. The oxidation process is achieved according to Equation 8 and correspods to a weight gain $\Delta m/m_0$ depending on the oxidation rate and on the x value (Fig. 24)

$$SiO_{2x}N_{4(1-x)/3} + (1-x)O_2 \rightarrow SiO_2 + [2(1-x)/3]N_2 \quad (8)$$

It is well known that the high oxidation resistance of SiC and Si_3N_4 in a high oxygen partial pressure is strongly related to the formation of an oxide layer preventing an excessive diffusion of oxygen to the surface of the material and its subsequent oxidation (passive oxidation regime). The silica film resulting from the oxidation of the fibre remains smooth, dense, crack-free and adhesive up to $T_a = 1400\,°C$. Furthermore, the amorphous silica only starts to crystallize into cristobalite at 1400 °C as generally reported for pure SiC [25] but remains mainly amorphous after 10 h at this temperature. The thickness measured on different fibres as well as along the periphery of a given fibre is almost constant, indicating that oxidation was not locally enhanced by flaws from the fibre or the oxide layer (for instance, bubbles or cracks). The purity and the dense amorphous structure of the oxide layer up to high temperatures as well as the low viscosity and the expansion of the oxide layer during its formation (about 60 vol %) contribute to its tightness and consequently, to the high oxidation resistance of the fibres.

While the kinetics of oxidation of silicon and SiC is admitted to be controlled by the diffusion of molecular oxygen through the growing silica layer, Si_3N_4 oxidation kinetics is a subject of controversy [26–30]. Its exceptionally low oxidation kinetics would be related either to a complex diffusion/reaction regime [28] or to the formation of an intermediate silicon oxynitride layer between the silica and the Si_3N_4 [26, 27, 29, 30]. This material has been seldom and hardly evidenced by TEM and XPS analyses under the form of an amorphous silicon oxynitride with a composition varying continuously from SiO_2 to Si_3N_4 [30]. It is worthy of note that the local analysis of the oxide/fibre interface did not confirm the above feature but showed a steep chemical gradient.

5. Conclusion

The Si–N–O fibres grown by a CVD process consist of amorphous silicon oxynitride $SiO_{2x}N_{4(1-x)/3}$ with $0.1 < x < 0.2$. The composition and the yield of the fibres are thought to be governed by the formation and/or the providing of SiO and NH_3, and therefore strongly depend on the processing temperature and the ammonia flow rate. These fibres exhibit a large spread in tensile strength. The lowest values (about 1 GPa) correspond to large surface defects due to intergrowth while the highest values reach 5 GPa in perfect fibres. Despite their high oxygen content and their amorphous state, the fibres are remarkably stable up to 1500 °C under nitrogen. This feature is related to their high processing temperature (1450 °C) and the high nitrogen pressure preventing decomposition. Conversely, decomposition occurs under argon atmosphere, yielding free silicon and gaseous species (SiO and N_2) at 1450 °C, as predicted by thermodynamics. A preliminary study of the oxidation behaviour of the fibres showed that, similarly to SiC and Si_3N_4, their high oxidation resistance is mainly caused by the growth of a protective oxide layer. The present work shows the potential of these fibres to withstand high temperature applications in an oxidizing atmosphere as well as the severe conditions involved in CMC processing, e.g. in a reaction-bonded Si_3N_4 matrix.

Acknowledgements

This work has been supported through funding from the Swiss Priority Program for Materials Research. The authors are indebted to A. Klebe from the University of Bayreuth for the TEM and EELS investigations as well as R. Hany, R. Hauert and P. Boll from the EMPA, respectively for their advice and their assistance for the NMR, XPS and SEM analyses. They also gratefully thank H. Ewing and A. Vital from the EMPA for valuable discussions.

References

1. J. L. CHERMANT, "Les céramiques thermomécaniques" (CNRS éditions, Paris, 1989).
2. M. E. WASHBURN, *Amer. Ceram. Soc. Bull.* **46** (1967) 667.
3. K. OKAMURA, M. SATO and Y. HASEGAWA, *Ceram. Int.* **13** (1987) 55.
4. T. ISODA, "Controlled interphases in composite materials", edited by H. Ishida (Elsevier, New York, 1990) p. 255.
5. H. MATSUO, O. FUNAYAMA, T. KATO, H. KAYA and T. ISODA, *J. Ceram. Soc. Jpn* **102** (1994) 409.
6. D. BELITSKUS, "Fibres and whisker reinforced ceramics for structural applications" (M. Dekker Inc., New York, 1993).
7. V. N. GRIBKOV, V. A. SILAEV, B. V. SHCHETANOV, E. L. UMANTSEV and A. S. ISAIKIN, *Sov. Phys. Crystallogr.* **16** (1972) 852.
8. M. J. WANG and H. WADA, *J. Mater. Sci.* **25** (1990) 1690.
9. A. L. CUNNINGHAM and L. G. DAVIES, in Proceedings of the 15th SAMPE National Symposium and Exhibition, Los Angeles (Western Periodicals Co. and Society of Advanced Materials and Process Engineers, North Hollywood, CA, 1969) p. 209.
10. U. VOGT, H. HOFFMAN and V. KRAMER, *Key Engng Mater.* **89–91** (1994) 29.
11. U. VOGT, G. CHOLLON and K. BERROTH, in Proceedings of the 17th International SAMPE European Symposium, Basel, edited by U. Meier and M. A. Erath (SAMPE Europe, Niederglatt-Zuerich, 1996) p. 379.
12. R. DUPREE, M. H. LEWIS, G. LENG-WARD and D. S. WILLIAMS, *J. Mater. Sci. Lett.* **4** (1985) 393.
13. K. R. CARDUNER, R. O. CARTER, M. E. MILBERG and G. M. CROSBIE, *Anal. Chem.* **59** (1987) 2794.
14. R. MARCHAND and J. LANG, *C.R. Acad. Sci. Paris* **264**, Série C (1967) 969.
15. R. WUSIRIKA, *J. Amer. Ceram. Soc.* **73** (1990) 2926.
16. R.VAN WEEREN, E. A. LEONE, S. CURRAN, L. C. KLEIN and S. C. DANFORTH, *ibid.* **77** (1994) 2699.
17. J. SJOBERG and R. POMPE, *ibid.* **75** (1992) 2189.
18. Y. MISUHARA, M. NOGUSHI, T. HISHIHARA and Y. TAKITA, *ibid.* **78** (1995) 109.
19. D. LIN and S. KIMURA, *ibid.* **79** (1996) 2947.
20. A. H. HEUER and V. L. LOU, *ibid.* **73** (1990) 2789.
21. S. C. SINGHAL, *Ceram. Int.* **2** (1976) 123.
22. J. HOJO, H. MAEDA and A. KATO, *Sramikkusu Ronbunshi* **96** (1988) 842.

23. K. BLEGEN, "Special ceramics" **6**, edited by P. Popper (British Ceramic Research Association, Stoke on Trent, 1975) p. 223.
24. P. ROCABOIS, Doctoral Thesis, Institut National Polytechnique de Grenoble (1993).
25. J. A. COSTELLO and R. E. TRESSLER, *J. Amer. Ceram. Soc.* **64** (1991) 327.
26. H. DU, R. E. TRESSLER, K. E. SPEAR and C. G. PANTANO, *J. Electrochem. Soc.* **136** (1989) 1527.
27. H. DU, R. E. TRESSLER and K. E. SPEAR, *ibid.* **136** (1989) 3210.
28. K. L. LUTHRA, *ibid.* **138** (1991) 3001.
29. L. U. T. OGBUJI and J. L. SMIALEK, *ibid.* **138** (1991) L51.
30. L. U. T. OGBUJI and D. T. JAYNE, *ibid.* **140** (1993) 759.

Received 10 March
and accepted 23 October 1997